Peptide Hydrolysis Catalyzed by Matrix Metalloproteinase 2: A Computational Study

Dr. Natalia Díaz* and Dr. Dimas Suárez

Departamento de Química Física y Analítica, Universidad de Oviedo. C/ Julián Clavería, 8, 33006, Oviedo (Asturias), Spain

Received: April 22, 2008

The MMP-2 reaction mechanism is investigated by using different computational methodologies. First, quantum mechanical (QM) calculations are carried out on a cluster model of the active site bound to an Ace−Gly∼Ile−Nme peptide. Along the QM reaction path, a Zn-bound water molecule attacks the Gly carbonyl group to give a tetrahedral intermediate. The breaking of the C−N bond is completed thanks to the Glu_{404} residue that shuttles a proton from the water molecule to Ile−N atom. The gas-phase QM energy barrier is quite low (∼14 kcal/mol), thus suggesting that the essential catalytic machinery is included in the cluster model. A similar reaction path occurs in the MMP-2 catalytic domain bound to an octapeptide substrate according to hybrid QM and molecular mechanical (QM/MM) geometry optimizations. However, the rupture of the Gly(P_1)∼Ile(P_1') amide bond is destabilized in the static QM/MM calculations, owing to the positioning of the Ile(P_1') side chain inside the MMP-2 S_1' pocket and to the inability of simple energy miminization methodologies to properly relax complex systems. Molecular dynamics simulations show that these steric limitations are overcome easily through structural fluctuations. The energetic effect of structural fluctuations is taken into account by combining QM energies with average MM Poisson−Boltzmann free energies, resulting in a total free energy barrier of 14.8 kcal/mol in good agreement with experimental data. The rate-determining event in the MMP-2 mechanism corresponds to a H-bond rearrangement involving the Glu_{404} residue and/or the Glu_{404}−COOH → N−Ile(P_1') proton transfer. Overall, the present computational results and previous experimental data complement each other well in order to provide a detailed view of the MMPs catalytic mechanism.

Introduction

Matrix metalloproteinases (MMPs) are a family of structurally related, zinc- and calcium-dependent endopeptidases that catalyze the hydrolysis of virtually all kinds of extracellular matrix proteins. This hydrolytic activity is central in those physiological processes that require tissue turnover and remodelling. However, overexpression of several MMPs occurring in various inflammatory, malignant, and degenerative diseases, converts these enzymes in potential drug targets.[1–5] Current efforts in the field pursue to develop more selective compounds designed to target only the MMPs involved in a given pathology.[6–9] In this context, further knowledge of the structure, dynamics, and function of the target enzymes will probably help in the rational design of improved inhibitors.

The MMPs are multidomain proteins composed, in most cases, of an *N*-terminal prodomain, a catalytic domain, and a *C*-terminal hemopexin-like domain.[10] The crystal structures available for these enzymes show that the catalytic domain invariantly displays three α-helices, a five-stranded β-sheet, and a number of loops. The enzymatic active site is a shallow cleft that extends horizontally across the catalytic domain. According to previous results, peptide substrates align in this cleft by establishing H-bond contacts with several main-chain groups from the β4-strand and the Ω-loop, whereas the side chains of the substrate interact with the so-called S_3−S_3' sites of the catalytic domain.[10,11] In the central region of the active site groove, a catalytic zinc ion (Zn_1) is bound by three histidines from a conserved zinc binding motif (HEXXHXXGXXH) and a varying number of water molecules (1−3) in the mature enzyme.[12,13] One of these water molecules (Wat_1) remains H-bonded to the invariant glutamate residue adjacent to the first histidine in the Zn_1-binding motif.

Most of the kinetic analyses performed for the MMPs have employed peptide phage libraries to identify the substrate selectivity of the enzymes in terms of recognition (K_m) and catalysis (k_{cat}). These kinetic studies have shown that the MMPs hydrolyze their preferred peptide substrates with rate constants (k_{cat}) of 10^1−10^2 s^{-1}.[14–16] The pH dependence of MMP catalysis is bell-shaped with limiting pK_a values of 4−6 and 8−10, depending on the enzyme and the substrate considered.[17–19] The acidic pK_a value was initially assigned to the conserved active-site glutamate that would play a role as a general base catalyst.[19] Mutagenesis experiments performed for several MMPs have confirmed the relevance of this residue during catalysis. Thus, the conservative Glu → Asp substitution drastically reduces the k_{cat}/K_m values (10−24% of that of the wild-type enzyme) for the hydrolysis of peptide substrates.[20–22] Even a lower activity (0.01−0.6% of that of the wild-type enzyme) is observed for the Glu → Gln and Glu → Ala mutants in several MMPs. However, the pH dependence of the k_{cat}/K_m values measured for these Glu mutants in MMP-7 is also bell-shaped, with limiting pK_a values similar to those observed for the wild-type enzyme.[18] Clearly, this result contradicts the assignment of the acidic pK_a value to the active-site Glu residue. Other proposals ascribe the low limit of the pH dependence of k_{cat}/K_m to the zinc-bound water molecule, with Glu playing an important role in catalysis because of the stabilization of the rate determining transition structure, or to the protonation of the leaving amino group.[18]

* Corresponding author. Phone: +34-985103492. FAX: +34-985103125. E-mail: diazfnatalia@uniovi.es.

10.1021/jp803509h CCC: $40.75
Published on Web 06/21/2008

SCHEME 1: Proposed Reaction Mechanism (X = Glu for Thermolysin and X = His for the MMPs)

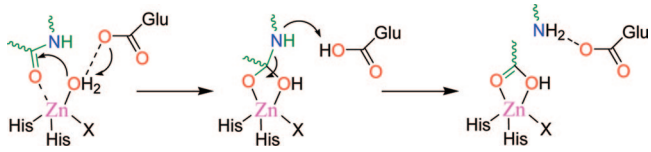

The MMPs are distantly related to the thermolysin family of metalloproteinases. They share some structural features and a limited active-site motif (HEXXH), which suggests that the two enzymes could present a similar mechanism of catalysis.[10,23] The traditionally accepted mechanism for thermolysin displays a zinc-bound water molecule that is activated for nucleophilic attack by the catalytic glutamate which, in turn, shuttles a proton to the leaving amino group (see Scheme 1).[24] Interestingly, this mechanism also finds experimental support for the MMPs in the above-mentioned kinetic studies and in different crystallographic analyses. The crystal structures of MMPs bound to different hydroxamate inhibitors show that the carboxylate group of the glutamate interacts with the oxygen and nitrogen atoms of the hydroxamate moiety that mimic the nucleophilic water molecule.[25] Moreover, Bertini et al. have obtained crystal structures for the corresponding product structure with one or two hydrolysis fragments located in the active site cavity.[12] The contacts observed in these structures are compatible with the role assigned to the conserved glutamic acid. Nevertheless, many details of the reaction mechanism remain to be elucidated.

Clearly, a detailed picture of the peptide hydrolysis catalyzed by the MMPs requires the determination of both structural and energetic data for the Michaelis complex, transition structures, and reaction intermediates. In principle, such mechanistic knowledge can be obtained from quantum mechanical (QM) calculations aimed at determining the relevant critical points on the potential energy surface (PES). For the MMPs, only one theoretical study of the reaction mechanism has been reported, modeling the hydrolysis of *N*-methyl-acetamide in the presence of a significantly reduced model of the MMP-3 enzyme.[26] The authors characterize a one-step mechanism in which the conserved glutamic acid shuttles a proton from the metal-bound water molecule to the leaving amino group of the peptide substrate. The transition structure is dominated by the formation of the C−O bond through nucleophilic attack, determining a free energy barrier of about 13 kcal/mol. However, the authors have pointed out that their model might not be valid to study the last events of the hydrolysis reaction (i.e., proton transfer to the leaving amino group and breaking of the peptide C−N bond), because motion of the amine part of the cleaved peptide would be partially restricted in the actual enzyme.

In previous theoretical work, we have examined some structural aspects of the catalytic domain of the MMP-2 enzyme. This enzyme, also termed gelatinase A, is a key player in angiogenesis, and its expression has been observed in a number of tumors.[4,27,28] For this system, QM and hybrid QM/molecular mechanics (QM/MM) calculations confirmed that the Zn_1 ion in the active site presents a flexible coordination sphere in which one hydroxide anion or two or three water molecules can bind to the metal ion in the active (unbound) form of the enzyme.[13] Subsequently, we have investigated the role played by the so-called structural metal ions (calcium and zinc) in the MMP-2 catalytic domain. By means of molecular dynamics (MD) simulations and free energy calculations, we have found that the enzyme configuration with two calcium and two zinc ions is the thermodynamically most stable one and that all the important binding sites are readily accessible in such configuration.[29] For the MMP-2 catalytic domain, we have also examined the positioning of its *N*-terminal coil,[11] which is related to a phenomenon called superactivation.[30] The simulations confirm that the position of the *N*-terminal coil observed in the superactivated forms of other MMPs is also favored in the MMP-2 enzyme. Substrate binding have been modeled by using a peptide with the sequence Ace−Gly−Pro−Gln−Gly∼Ile−Ala−Gly−Gln−Nme (**Pα1**) that corresponds to the α1 chain of collagen type I around the peptide bond that is specifically hydrolyzed by the MMPs.[31] The MD calculations point out that **Pα1** binds to MMP-2 in an extended conformation, which is stabilized by several H-bond contacts (see Scheme 2) and that the Zn_1-bound Wat_1 molecule is properly oriented for nucleophilic attack.[11] Therefore, our previous studies on the MMP-2 catalytic domain have converged in an atomic model of the Michaelis complex formed between the MMP-2 enzyme and the **Pα1** substrate that is best suited to computationally investigate the reaction mechanism for the hydrolysis of the Gly(P_1)∼Ile(P_1') peptide bond.

SCHEME 2: Main Enzyme/Substrate Contacts

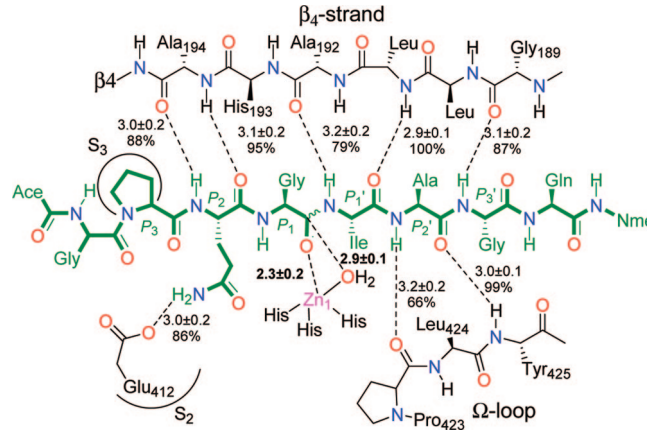

In this work, we investigate the reaction mechanism catalyzed by MMP-2 by using different computational techniques and molecular models in order to examine the actual impact of different factors affecting the catalytic process. First, we reinvestigated the hydrolysis reaction in a relatively small model by using a QM method. Subsequently, we took into account the rest of protein and solvent environment by means of hybrid QM/MM calculations. Thus, two QM/MM reaction profiles were determined, starting at different snapshots extracted from our MD simulation of the MMP-2/**Pα1** complex. Finally, we estimated free energy contributions due to structural fluctuations of the surrounding protein and solvent environments. This was accomplished by building MM representations of the reactive MMP-2 region that were used in MD simulations followed by molecular-mechanics-Poisson−Boltzmann (MM-PB) calculations. By combining the QM energy of the reactive structures along the static QM/MM reaction profiles with the average MM-PB energies, we estimated the free energy of the reactive structures in the enzyme. Altogether, our theoretical results provide a detailed molecular description of the peptide hydrolysis reaction that takes place at the active site of the MMP enzymes. These results could provide some useful tips for the rational design of novel MMP inhibitors.

Experimental Methods

QM Calculations. The cluster model of the active site was built by including the side chains of residues His_{403}, Glu_{404},

His_{407}, and His_{413}, the Zn_1 ion, the nucleophilic Wat_1 molecule, and a short Ace−Gly∼Ile−Nme peptide substrate (1CK7 numbering).[32] Coordinates were taken from a representative snapshot of our previous MD simulation study.[11] For comparative purposes, the same QM level of theory was employed in the gas-phase cluster and in the QM/MM optimizations in the enzyme. Thus, the QM calculations were carried out by using the B3LYP density functional with the double-ζ 6-31G* basis set for nonmetal atoms[33] and the Los Alamos effective core potentials for zinc[34] (this mixed basis set is usually denoted as LACVP*). As shown in the Supporting Information, comparison of DFT and high-level ab initio calculations on a small system (*N*-methylacetamide reacting with a $[Zn(NH_3)_3(OH)]^+ \cdot H_2O$ complex) indicates that the B3LYP/LACVP* level of theory can yield reasonable structures and energy barriers for the enzymatic hydrolysis reaction studied in this work.

Geometry optimizations of the cluster models of the active site at the B3LYP/LACVP* level were carried out with the Jaguar program.[35] To prevent the movement of groups of atoms to locations unattainable in the MMP-2 system, the cluster models were optimized with constraints. For the His_{403}, Glu_{404}, His_{407}, and His_{413} moieties included in the cluster model, constraints were imposed by including the three closest backbone heavy atoms as dummy atoms. All bonds, angles, and dihedrals formed with these dummy atoms were fixed. Similar constraints were also imposed along the Ace moiety of the Ace−Gly∼Ile−Nme peptide (we note in passing that geometrical restrictions on the Ile−Nme backbone atoms were found to be incompatible with the peptide hydrolysis reaction). Transition structures were located by employing the synchronous transit quasi-Newton method implemented in Jaguar.

After geometry optimization, analytical frequency calculations were performed at the B3LYP/LACVP* level by using the Gaussian03 program[36] and the converged wave function from Jaguar. The Hessian matrix was then transferred to the Jaguar program in order to characterize the critical points and compute thermodynamic data at 298 K (the contribution of the residual gradient due to the constraints was removed from the Hessian matrix by using a simple projection operator). Single-point B3LYP/LACVP* self-consistent reaction field PB (SCRF-PB) calculations[37] were also carried out on the gas-phase QM geometries by using Jaguar. Several values for the dielectric constant of the surrounding continuum (ε) were considered to analyze the trend in the relative solvation energies.

QM/MM Calculations. Initial coordinates for the QM/MM systems were extracted from our previous MD simulation of the Michaelis complex formed between the MMP-2 catalytic domain and the **Pα1** peptide.[11] We selected two snapshots that were subject to MM minimization during 10 000 steps by using the same settings as in the MD simulation. Subsequently, a 25 Å solvent cap centered at the oxygen atom of Wat_1 was created. Thus, the resulting systems included the whole catalytic domain of MMP-2 with two Ca^{2+} and two Zn^{2+} ions bound to the enzyme, the **Pα1** octapeptide, and 1702 water molecules.

QM/MM geometry optimizations were carried out by using the version 6.0 of the QSite program.[38] QM-MM interfaces were placed at the His_{403}−Cα−N, Phe_{405}−N−Cα, His_{407}−Cβ−Cα, and His_{413}−Cβ−Cα bonds of MMP-2 and the Gln(P_2)−C−Cα and the Ala(P_2')−N−Cα bonds of the peptide substrate. In addition, the QM region also included the catalytic Zn_1 ion and Wat_1. This partitioning resulted in a QM region comprising a total of 94 QM atoms with a net charge of +1 that was described at the B3LYP/LACVP* level of theory (841 basis functions). The rest of the protein and solvent atoms were treated with the OPLS-AA force field.[39] We note that the B3LYP/LACVP* level of theory together with the OPLS force field have been specifically optimized for modeling protein active sites, with parametrization enabling the QM region to be defined via a series of cuts in the backbone and at side chains between Cα and Cβ atoms.[40]

During QM/MM geometry optimizations, all the protein residues that contact the QM region were allowed to move. These included Leu_{190}−Ala_{194}, Val_{400}, His_{403}−His_{407}, Glu_{412}, His_{413}, and Ala_{422}−Tyr_{425}. In addition, Zn_1, the whole **Pα1** peptide, and the closest 50−52 water molecules were relaxed. The position of the rest of the protein and solvent molecules was frozen during the QM/MM calculations. Minimizations were performed with no cutoff until the root-mean-squared residual gradient was less than $5.0\ 10^{-4}$ au, permitting thus a proper relaxation of the QM region, the proximal protein, and solvent residues.

Long-range solute−solvent electrostatic interactions were estimated by means of PB calculations after having deleted the coordinates of the majority of the MM water molecules in the optimized QM/MM structures (only the 50 water molecules that are the closest to the Zn_1 atom were kept). Single-point QM/MM calculations were also carried out on the same structures to give the $E_{QM/MM}^{enzyme}$ energies. The PB solvation free energy (G_{PB}) was determined by using the Delphi program.[41] The protein was represented as a low dielectric continuum (a value of $\varepsilon_{int} = 1$ was used in the calculations) with embedded charges and the solvent as a high dielectric continuum ($\varepsilon_{out} = 80$) with no salt. The OPLS-AA atomic charges were used for the protein atoms excepting those atoms that were within the QM region during QM/MM geometry optimizations. For these atoms, we used their ESP charges derived from single-point B3LYP/LACVP* calculations on the QM region of the corresponding QM/MM optimized geometries after having placed H-link atoms at the QM/MM cuts (a zero value to the atomic charges of the H-link atoms was assigned in the ESP fitting procedure by using the RESP program[42]).

MD, MM, and PB Calculations. In order to estimate the free energy profile for the MMP-2 reaction, both long-range electrostatic effects as well as structural fluctuations of the surrounding protein and solvent environments must be taken into account. The QM and QM/MM calculations show that the essential structural features of the reacting points along the MMP-2 mechanism are quite invariant with respect to the nature of their environment. We therefore decided to use approximate free energy methodologies in order to estimate free energy corrections to the static QM/MM energy profiles. Note that conventional free energy perturbation calculations along a predefined reaction coordinate[43,44] would have been difficult to converge and very expensive computationally for the MMP-2 reaction mechanism. Thus, we computed free energy corrections by combining MM and PB calculations carried out on a statistical ensemble of enzyme/substrate structures. These structures are generated by means of classical MD simulations performed with the locally-enhanced sampling (LES) technique[45] and with geometric constraints that fix the active region of the enzyme at a given value of the reference QM/MM reaction coordinate. We note that the same strategy, which can be considered a variant of the so-called MM-PB approach,[46] has been applied successfully to investigate the mechanisms of the deacylation reaction in the active site of human butyrylcholinesterase, the intramolecular S_N2 reaction in water of a phenol succinate monoester, and the conversion of (−)-chorismate to prephenate catalyzed by the chorismate mutase enzyme.[47] We

also note that a similar approach has been proposed by Warshel and co-workers[48] by using the electron valence bond method as a reference potential and then using the linear response approximation and geometrical constraints at the transition state (TS).

To apply the MM-PB approach on the QM/MM reaction profiles, we combine the QM energy of the reactive region (i.e., the QM region adopted in the QM/MM calculations) with average MM-PB free energies. Thus, for example, the relative free energy of a TS structure in the enzyme was estimated by the following equation

$$\Delta G = E_{QM}(TS) - E_{QM}(react) + \Delta\bar{G}_{MMPB} \quad (1)$$

where the E_{QM} terms are the QM energies of the corresponding reactive region of the TS and reactant structures and $\bar{\Delta}G_{MMPB}$ represents the average environmental correction to ΔE_{QM} that is obtained through the following expression

$$\Delta\bar{G}_{MMPB} = \bar{G}^{enzyme}_{MMPB}(TS) - \bar{G}^{enzyme}_{MMPB}(react) \quad (2)$$

where the $\bar{G}^{enzyme}_{MMPB}$ terms are the average MM-PB free energies of the corresponding TS and reactant enzyme/substrate complexes but excluding the MM energy contributions arising from interactions among the reactive atoms. The average free energy terms ($\bar{G}_{MMPB}$) in eq 2 are computed by combining MM and PB electrostatic calculations

$$\bar{G}_{MMPB} = \bar{E}_{MM} + \bar{G}_{PB} \quad (3)$$

where $\bar{E}_{MM}$ is the average molecular mechanical energy and $\bar{G}_{PB}$ is the solvation free energy obtained by PB electrostatic calculations. Note that harmonic entropic contributions of the surroundings are not taken into account.

Setting Up the MM-PB Calculations. For each of the two QM/MM energy profiles, we performed a MD-LES simulation in which the reactive MMP-2 region is described by multiple LES copies (these copies do not interact with each other and interact with the rest of the system in an average way). The usual implementation of the LES algorithm assumes that all the copies share the same topology and atomic charges (i.e., the same covalent structure). In our approach, however, each LES copy corresponded to a reactive MM model with a particular set of atomic charges. In addition, we constrained the internal geometry of the LES copies by adding a harmonic energy term computed from the rms coordinate deviations (rmsd) between each copy in the simulation and its reference QM geometry.

Atomic partial charges for the reactive MM models were derived from the B3LYP/LACVP* electrostatic potential of the corresponding QM regions in the optimized QM/MM structures. We employed the RESP fitting methodology[49] in order to assign a zero value to the atomic charges of the H-link atoms and to fix the net charge of the QM atoms that are not involved in the bond forming/breaking processes to their equivalent values in the standard AMBER database. In this way, we made sure that electrostatic interactions between all atoms of the enzymatic system are treated on an equal basis, thereby minimizing partial charge artifacts in the MM-PB calculations. The set of atom types in the MM representation of the Michaelis complex was used for all the reactive MM models.

Starting at the selected snapshots from our previous MD simulation, a 5.0 ns MD-LES simulation was carried out with five different LES copies of the reactive MM models: the first pre-reactive complex (**C**$_1$), the three intermediates (**I**$_1$, **I**$_2$, and **I**$_3$), and the product complex (**P**). The geometry of each LES copy was linked to its corresponding QM reference structure by applying appropriate rmsd constraints. The simulations were run with protocols identical to those previously used for the MMP-2 enzyme.[11] All the MD trajectories were computed with the SANDER module of the AMBER 9.0 package of programs.[42]

One hundred snapshots were extracted from the last 2500 ps of each MD-LES trajectory. The snapshots were processed before carrying out the MM-PB calculations by removing the counterions and most of the waters. Only the ~50 water molecules closest to the Zn_1 atom were kept because these interact directly with the reacting atoms. The coordinates of the LES copies were replaced by those of the reactive MM models along the energy profile. In this way, we generated 10 structures, differing only in the coordinates of the reactive MM model, from a single MD-LES snapshot. This task was accomplished by rigid superposition of the different reactive MM models onto selected backbone atoms of the MD-LES snapshot, followed by partial MM relaxation of the explicit solvent molecules and the residues adjacent to the reactive MM model.

The MM and PB calculations were done with AMBER charges for the different models. All the MM energies were computed with no cutoff by using the SANDER program.[42] The PB calculations were carried out with the program Delphi, by solving the linearized PB equation on a cubic lattice by using an iterative finite-difference method (1000 iterations), a grid spacing of 0.5 Å (200 × 200 × 200), and DREIDING van der Waals radii for C, H, N, O, and S atoms.[50] The dielectric boundary was the contact surface between the radii of the solute and the radius (1.4 Å) of a water probe molecule. The Debye−Huckel approximation was used to determine the potentials at the boundary of the grid.

Results and Discussion

Minimal Model for MMP-2 Catalysis: Gas-Phase QM Calculations. Figure 1 shows the B3LYP/LACVP* critical structures involved in the hydrolysis of the small Ace−Gly~Ile−Nme peptide catalyzed by the cluster model of the MMP-2 active site. Detailed information including absolute and relative energies, thermal corrections, and solvation free energies are collected in the Supporting Information (Table S2).

Altogether the critical structures collected in Figure 1 depict a catalytic mechanism for peptide hydrolysis that basically consists of an initial nucleophilic attack of a Zn-bound hydroxide to the substrate carbonyl group, followed by proton transfer to the leaving amino group from the protonated Glu_{404} side chain. The main structural and energetic features of the mechanism are as follows. For the pre-reactive complex, the proton tautomer that minimizes charge separation (**^{QM}C**) is the only stable energy minimum on the gas-phase B3YP/LACVP* PES. In this structure, the Zn_1-bound hydroxide is properly positioned for nucleophilic attack toward the Zn_1-coordinated carbonyl group of the peptide substrate, whereas the carboxylic Glu_{404} group is H-bonded to the Zn−OH fragment (see Figure 1). At the TS for nucleophilic attack (**^{QM}TS$_1$**), the formation of the C−O bond is quite advanced (1.77 Å), but its energy barrier is quite low (10.1 kcal/mol). This structure is connected with a zinc-bound tetrahedral intermediate (**^{QM}I$_1$**), which is only 1.7 kcal/mol below **^{QM}TS$_1$**. Ongoing from the pre-reactive complex **^{QM}C** to **^{QM}I$_1$**, the −Ile−Nme fragment of the peptide substrate approaches the Glu_{404} carboxylic group, and the Ile−N atom becomes partially pyramidalized. The shift motion of the peptide substrate is required for the N atom of the Gly~Ile peptide linkage to form an Ile−N···HO−Glu_{404} H-bond contact at a distance of 3.30 Å between heavy atoms. In turn, this interaction

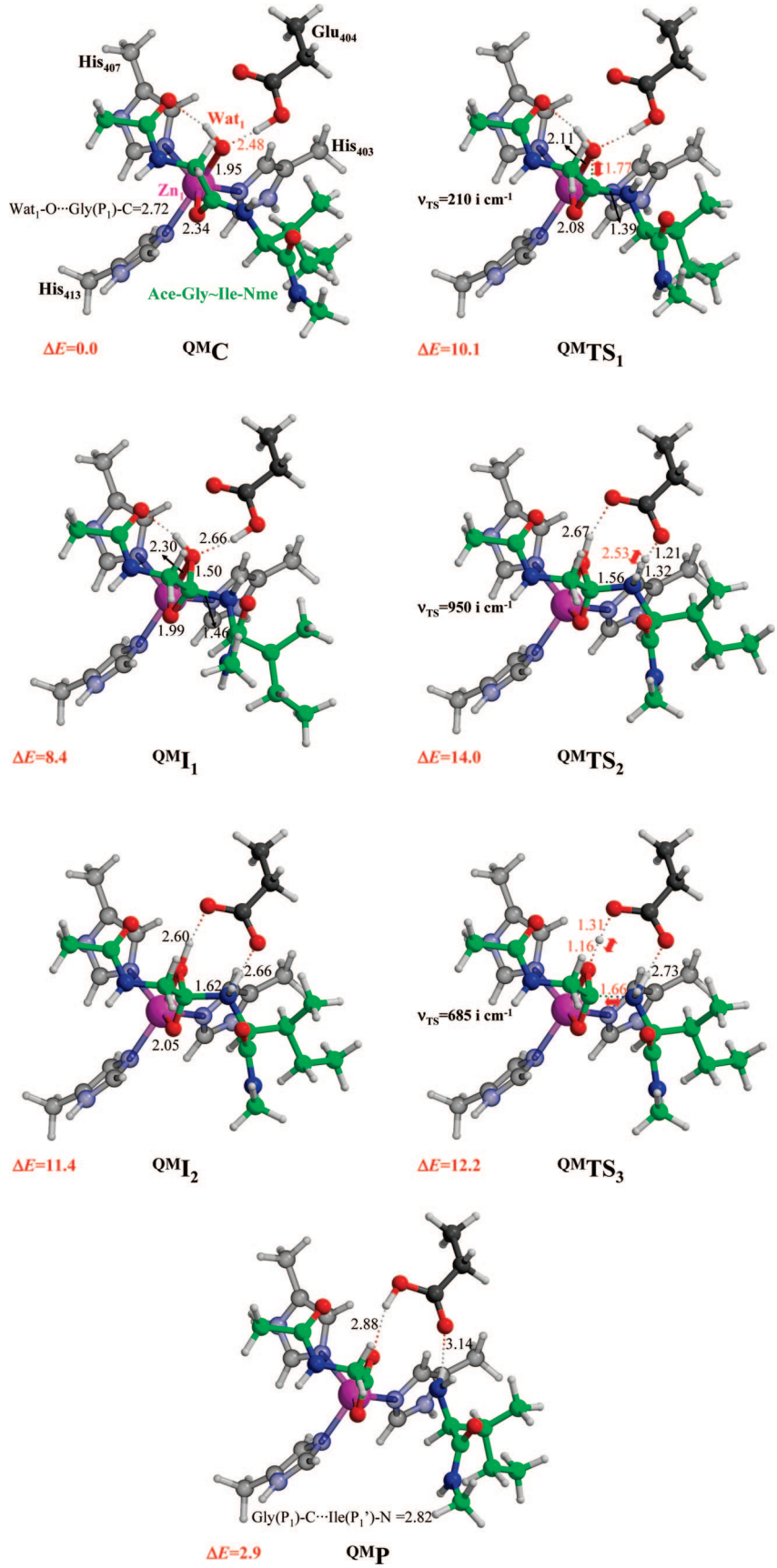

Figure 1. Optimized structures for the hydrolysis of Ace−Gly∼Ile−Nme in a cluster model of the MMP-2 active site. Relative energies are given in kcal/mol and distances are in Angstroms.

is essential for the protonated Glu_{404} to donate its proton to the Ile−N atom through the $^{QM}TS_2$ structure, leading to a second tetrahedral intermediate $^{QM}I_2$ which is 3.0 kcal/mol less stable than $^{QM}I_1$. The transition vector of $^{QM}TS_2$ is dominated by the Glu_{404}−OH → :N−Ile proton transfer, its relative energy being 14.0 kcal/mol (see Figure 1). In addition, an umbrella inversion of the

Zn−OH−C moiety takes place during the $^{QM}\mathbf{I_1} \rightarrow {}^{QM}\mathbf{I_2}$ process. As a consequence, the Zn−OH···O=C−Ace hydrogen bond at $^{QM}\mathbf{I_1}$ evolves into a short Zn−OH···$^{-}$OOC−Glu_{404} contact at $^{QM}\mathbf{I_2}$. In fact, proton transfer from the Zn−OH moiety to the negatively charged carboxylate group triggers the rupture of the C−N single bond at $^{QM}\mathbf{I_2}$. Thus, the $^{QM}\mathbf{TS_3}$ structure, which is only 0.8 kcal/mol above the $^{QM}\mathbf{I_2}$ structure, is characterized by a transition vector that exhibits simultaneous proton transfer with a small elongation of the C−N bond. At the corresponding product complex ($^{QM}\mathbf{P}$ in Figure 1), the catalytic Zn_1 atom is coordinated in a bidentate manner by the Ace−Gly−COO^- group, whereas the amino group of the NH_2−Ile−Nme fragment is H-bonded to the Glu_{404} and gives a weak donor−acceptor interaction with the Ace−COO^- group.

Clearly, the gas-phase reaction path shown in Figure 1 is a convenient first step in the computational investigation of the catalytic mechanism of the MMP-2. Perhaps, its most interesting features are (a) the flatness of the PES around the tetrahedral intermediates $^{QM}\mathbf{I_1}$ and $^{QM}\mathbf{I_2}$ that is hardly altered by addition of thermal corrections and/or inclusion of environment polarity effects (see Table S2 in the Supporting Information), (b) the shift motion of the Ile−Nme fragment, which is required for the proton transfer and the rupture of the peptide bond, and (c) the relatively low values of the rate-determining energy barrier (∼15 kcal/mol) for proton transfer from Glu_{404} to the Ile−N atom, which suggests that the essential catalytic machinery for hydrolysis is already provided by the $[Zn(imidazol)_3OH]^+$ complex and the Glu_{404} residue. Nevertheless, further energy calculations on the solvated enzyme/substrate complex are also required to find out the actual mechanistic role of the rest of the enzyme and peptide substrate.

Selection of the Enzyme/Substrate Complexes for QM/MM Calculations. According to our previous MD simulation of the Michaelis complex formed between the MMP-2 catalytic domain and the **Pα1** substrate, several residues of **Pα1** give perfectly stable H-bond contacts with the important anchorage sites located across the MMP-2 active site region (see Scheme 2).[11] In addition, hydrophobic contacts enhance substrate binding as does that formed between the Leu(P_1') side chain and the S_1' hydrophobic pocket in the vicinity of Zn_1. During the simulation, the catalytic Zn_1 ion is covalently linked to the three conserved histidine residues and to a water molecule (Wat_1), which in turn is H-bonded to the Glu_{404} carboxylate. However, the Zn_1 ion also contributes to bind **Pα1** given that the carbonyl group of the Gly(P_1) residue acts as the fifth ligand around Zn_1, the average Gly(P_1)−O···Zn_1 distance being 2.31 ± 0.16 Å (this bond was not explicitly defined in the force-field representation of Zn_1).

In terms of the stability and nature of the enzyme/substrate contacts, all the MMP-2/**Pα1** structures generated by the MD simulation can be seen as pre-reactive configurations in which the **Pα1** substrate and the nucleophilic Zn_1-bound Wat_1 molecule have a relative orientation favorable for the initial nucleophilic attack to occur. Thus, all along the MD simulation, the Gly(P_1)−C···O−Wat_1 distance fluctuates moderately (±0.10 Å) around a mean value of 2.87 Å. Notwithstanding, solvent structure nearby the carbonyl group of the scissile peptide bond exhibits some variability that could be relevant for catalysis. On one hand, the Gly(P_1)∼Ile(P_1') residues of **Pα1** are hardly solvent accessible as shown by the radial distribution function on the Gly(P_1)−O atom which peaks at 4.2 Å and integrates to three water molecules up to 4.9 Å. It also shows a small shoulder at around 2.8 Å that integrates to ∼0.1 water molecules. On the other hand, a Gly(P_1)−O···H_2O···O−Pro_{423} water bridge is present in 4.2% of the analyzed snapshots with average O−O distances of 3.8 and 3.1 Å, respectively. The free energy of water bridge formation (ΔG_{bridge}) can be directly calculated from the probability (P) of bridge formation expressed as

$$\Delta G_{bridge} = -RT \ln P$$

Thus, the free energy cost of the one-water-molecule Gly(P_1)···Pro_{423} bridge amounts to only 1.9 kcal/mol. Because the presence of water molecules interacting directly with the Zn_1-bound carbonyl group could presumably stabilize transition structures and intermediates for peptide hydrolysis and the estimated ΔG_{bridge} is not large, we selected two different snapshots from the MD simulation of the MMP-2/**Pα1** complex in order to perform the QM/MM calculations with different starting environments. In one of these snapshots, which will be labeled as A, a water molecule interacts simultaneously with the carbonyl groups of Pro_{423} and Gly(P_1). This contact is absent in the second frame denoted as B, which represents the most likely solvent structure around the reactive site.

QM/MM Calculations: First Assessment of Solvent and Protein Effects. By starting at the selected A−B enzyme/substrate configurations, hydrolysis of the **Pα1** peptide was investigated by means of QM/MM geometry optimizations taking into account the whole MMP-2 catalytic domain hydrated by a large water cap centered on the Wat_1−O atom. In Figure 2, we show details of the structures optimized for the A reaction profile. The corresponding structures for the B pathway are displayed in Figure S2 in the Supporting Information, and the main geometrical information for the two profiles is collected in Tables S3−S4 in the Supporting Information. To better characterize the mechanistic influence of the solvent and protein environment, the QM/MM results will be discussed in reference to the above-described gas-phase QM calculations on the minimal MMP-2 model. Thus, we will focus first on the structural changes induced by the protein environment. Subsequently, we will analyze the corresponding energetic effects as estimated by single-point QM/MM, QM, and PB calculations on the optimized structures. Finally, we will comment on the similarities and differences among the two QM/MM reaction profiles.

Critical Points Located on the QM/MM PES. We note first that the two QM/MM reaction profiles predict the same molecular mechanism for peptide hydrolysis, which is also very similar to that obtained for the small QM cluster model. After the Zn-bound water molecule attacks the Gly(P_1) carbonyl group to give a tetrahedral intermediate, the breaking of the C−N bond is completed thanks to Glu_{404} that shuttles a proton from the Wat_1 molecule to the leaving amino group. It is equally important to note that Zn_1 remains penta-coordinated by the three histidines, Wat_1 and the Gly(P_1) carbonyl group adopting a distorted trigonal-bipyramid geometry all along the reaction coordinate (see Table S3 in the Supporting Information). Nevertheless, the exploration of the PES by the QM/MM calculations resulted in new structural features that were not observed in the previous QM cluster calculations. In the following discussion, we provide the range of values observed across the two pathways for selected distances and angles.

Two different pre-reactive complexes ($\mathbf{C_1}$ and $\mathbf{C_2}$) are located on the QM/MM PES (see Figure 2). The $\mathbf{C_1}$ complex presents a Zn_1−OH_2···Oε2−Glu_{404} interaction as in the MM representation used in the MD simulations. At the second complex, $\mathbf{C_2}$, Wat_1 donates a proton to the Glu_{404} side chain, resulting in a Zn_1−OH···HOε2−Glu_{404} H-bond. The two structures, $\mathbf{C_1}$ and $\mathbf{C_2}$, are characterized by a short OH···O H-bond distance

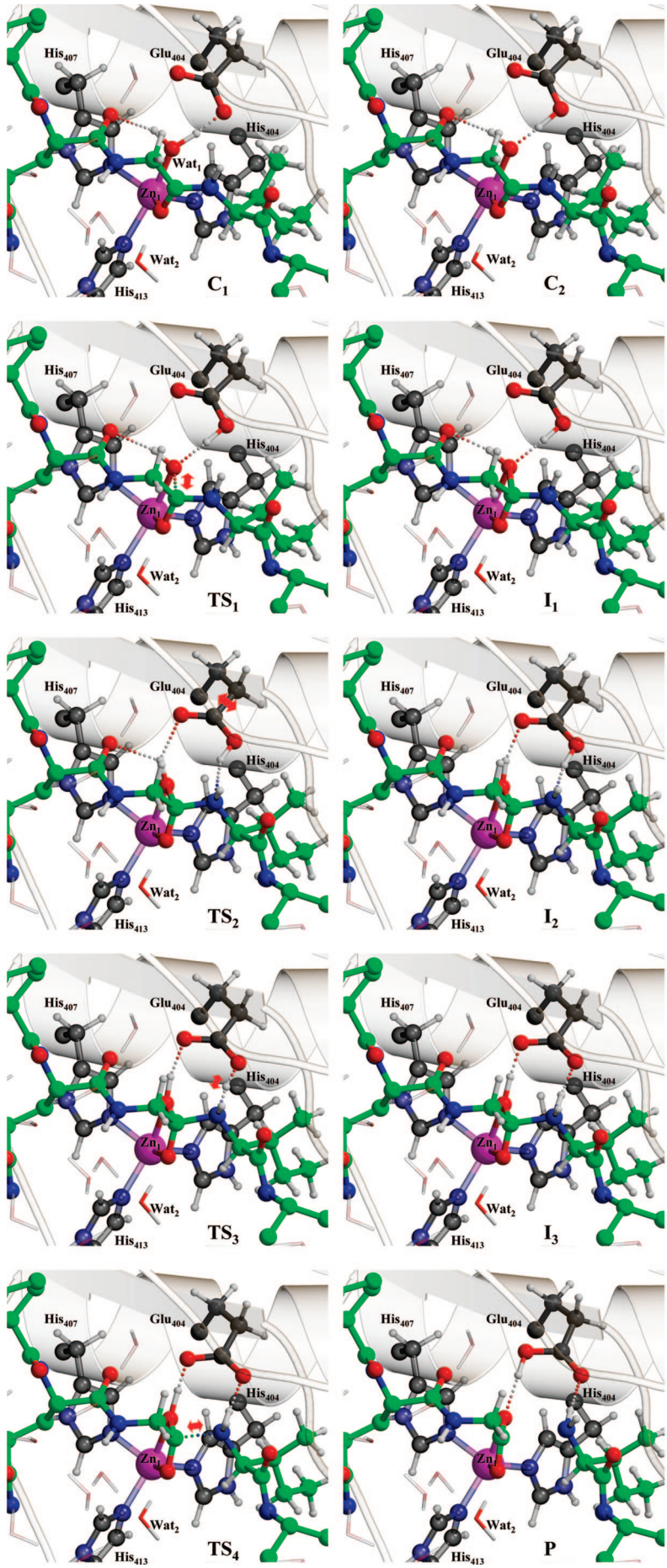

Figure 2. Optimized structures (configuration *A*) for the hydrolysis of **Pα1** in the catalytic domain of the MMP-2 enzyme.

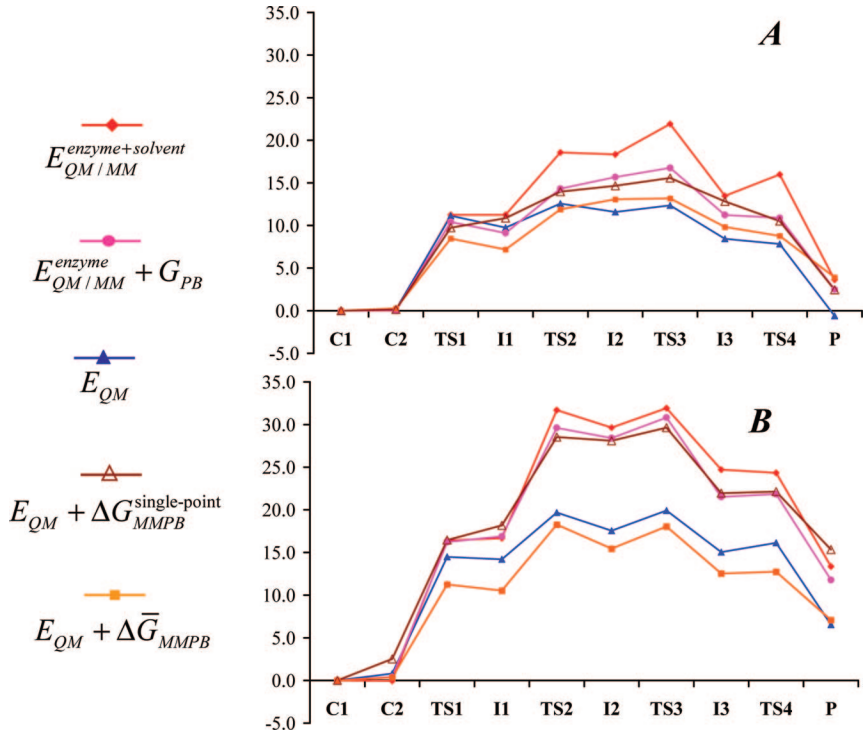

Figure 3. Energy profiles (in kcal/mol) for the hydrolysis of **Pα1** in the active site of the MMP-2 enzyme.

(1.3−1.4 Å) and a quite elongated O−H bond (1.1 Å). Wat_1 also interacts with the carbonyl group of Gln(P_2) from the peptide substrate, either in $\mathbf{C_1}$ and $\mathbf{C_2}$ (2.0−2.2 Å), a contact that contributes to properly orient the Wat_1−O lone pair toward the carbonyl group of the scissile peptide bond. Moreover, the binding of the Gly(P_1) carbonyl group to Zn_1 in both complexes (2.2−2.4 Å) results in a short Wat_1−O···C−Gly(P_1) distance (2.6−2.8 Å) for the nucleophilic attack. Overall, $\mathbf{C_1}$ and $\mathbf{C_2}$ are very similar, both structurally and energetically, with $\mathbf{C_1}$ being slightly favored by ∼1 kcal/mol (see below).

In the QM small model, the formation of the Gly−C···O−Wat_1 bond takes place with simultaneous pyramidalization of the Ile−N atom (see $^{QM}\mathbf{TS_1}$ in Figure 1). In the hydrated enzyme, however, these processes are described by two different transition structures. Thus, the nucleophilic attack from $\mathbf{C_2}$ proceeds through $\mathbf{TS_1}$ (Gly(P_1)−C···O−Wat_1 ≈ 1.7−1.9 Å) and leads to the *gem*-diolate intermediate $\mathbf{I_1}$ (Gly(P_1)−C···O−Wat_1 ≈ 1.6 Å). In the second step, the Ile(P_1')−N atom becomes pyramidalized, and the H-bond rearrangement required for Glu_{404} to act as a proton shuttle occurs: the Glu_{404}−Oε2H···O−Wat_1 and the Wat_1−OH···O−Gln(P_2) interactions present in $\mathbf{I_1}$ are replaced by new Glu_{404}−Oε2H···N−Ile(P_1') and Wat_1−OH···Oε1−Glu_{404} H-bonds, respectively (see the $\mathbf{I_2}$ and $\mathbf{TS_2}$ structures in Figure 2). The resulting tetrahedral intermediate, $\mathbf{I_2}$, is very close in structure and energy to the previous $\mathbf{TS_2}$.

Concerning the protonation of the forming amino group and the rupture of the C−N bond, both the gas-phase QM and the QM/MM optimizations give comparable bond distances and angles involving the reacting atoms. Thus, the QM/MM calculations show that a single transition structure for the Glu_{404}−Oε2H → N−Ile(P_1') proton transfer connects $\mathbf{I_2}$ with the $\mathbf{I_3}$ intermediate, in which the protonated Ile(P_1') amino group is still bonded to the Gly(P_1) residue (C−N distance of 1.6−1.7 Å). Further elongation of the C−N bond leads to the $\mathbf{TS_4}$ structure (C···N ≈ 1.8−1.9 Å), followed by proton transfer from the Wat_1−OH1 proton to the Glu_{404}−Oε1 atom resulting in the product complex **P**, in which the Zn_1 ion is coordinated by the carboxylate group in a bidentate manner and the Glu_{404} side chain is neutralized. The short Gly(P_1)−C···N−Ile(P_1') contact at **P** (2.5 Å) suggests that product release is far from being completed. With respect to the reference gas-phase QM calculations, the enzymatic environment modifies both the nature of the TS for the C−N rupture (which is mainly dominated by proton transfer in the gas phase) and, most interestingly, the positioning of the Ile residue. Although the gas-phase QM calculations show an important displacement of the Ile(P_1') residue during the latter stages of the reaction, this motion is largely dampened out in the QM/MM structures, given that the Ile(P_1') side chain is buried inside the S_1' pocket and the Ile(P_1') backbone groups are H-bonded to Ala_{192}−O and Leu_{191}−N (see Scheme 2 and Figure S3 in the Supporting Information).

QM/MM Energy Profiles. Figure 3 represents schematically the energy profiles for the A and B configurations as estimated by different computational protocols. Absolute and relative energies are reported in the Supporting Information (Table S5). As mentioned in the Experimental Methods section, all the enzyme residues and water molecules that contact the reactive QM region were relaxed during the QM/MM energy minimizations. Although this MM region was fully optimized for each optimization step in the QM region and attention was paid to keep the whole system in the same local valley during the course of the optimizations, the relatively large size of the MM region resulted in a small energetic noise in the QM/MM energy profiles produced by the differences in the MM energy contributions. This effect, together with the smoothness of the PES in the vicinity of the transition structures, explains that some of the QM/MM energies for transition structures lie slightly below those of the corresponding intermediates (see Figure 3 and Table S5 in the Supporting Information).

With reference to the gas-phase QM data summarized in Figure 1, the static QM/MM energy profiles in Figure 3 show that the protein and solvent environment plays a 2-fold role: (a) it makes the catalytic Zn_1 ion to easily adopt two different

trigonal bipyramid arrangements that are characterized by the $Zn_1-OH_2\cdots{}^-OOC-Glu_{404}$ (**C_1**) and $Zn_1-OH\cdots HOOC-Glu_{404}$ (**C_2**) interactions, respectively, and (b) it has (apparently) an anticatalytic effect given that the QM/MM energy barriers for the hydrolysis process are significantly larger than the gas-phase QM values. This latter effect is much less accentuated in the A profile, in which the Gly(P_1) carbonyl group interacts directly with one water molecule, than in the B profile, in which the first solvation shell around the Gly(P_1)−O atom is empty.

The fact that the two pre-reactive complexes in the enzyme, **C_1** and **C_2**, are structurally and energetically very similar is not entirely unexpected on the basis of our previous QM/MM calculations on the native form of the catalytic MMP-2 domain.[13] In the absence of the peptide substrate, a second water molecule can be placed in the apical position around the first coordination shell of Zn_1, but the two charge configurations, $Zn_1-OH_2\cdots{}^-OOC-Glu_{404}$ and $Zn_1-OH\cdots HOOC-Glu_{404}$, are nearly isoenergetic. Therefore, all the QM/MM calculations point out that the Glu_{404} residue is well tuned for acting as a proton shuttle and that the two protonation states of Glu_{404} would be populated both in the native and the complexed forms of the MMP-2 enzyme.

The QM/MM relative energies ($E_{QM/MM}^{enzyme+solvent}$; filled diamonds and red lines in Figure 3) show that inclusion of the enzymatic environment tends to destabilize by 5−15 kcal/mol the **TS_2** → **I_2** → **TS_3** → **I_3** → **TS_4** structures involved in the protonation of the Ile(P_1')−N atom and the rupture of the C−N bond, whereas the computed energy barriers for the initial nucleophilic attack remain more comparable with the gas-phase QM values. In the enzyme, the rate-determining step would correspond to the protonation of the Ile(P_1')−N atom passing through the **TS_3** structure with an energy barrier of 21.9 and 31.9 kcal/mol for the A and B configurations, respectively. Combining single-point PB calculations (G_{PB}) with single-point QM/MM energies ($E_{QM/MM}^{enzyme}$), computed after having removed most of the explicit water molecules, results in a moderate decrease of the energy barriers ($E_{QM/MM}^{enzyme} + G_{PB}$; filled circles and magenta lines in Figure 3). However, the energetic penalty associated to the protonation and rupture of the peptide bond remains equally important in the $E_{QM/MM}^{enzyme} + G_{PB}$ energies.

To better understand the environmental effects on the QM/MM energies, we carried out single-point QM calculations by using only the coordinates of the QM region complemented with H-link atoms. From the resulting ΔE_{QM} values for the A configuration, the QM region contributes 12.4 kcal/mol to the rate-determining QM/MM energy barrier (**TS_3**), whereas the rest of the protein and solvent environment further increases the energy barrier by 9.5 kcal/mol (i.e., $E_{QM/MM}^{enzyme+solvent} - \Delta E_{QM}$). The corresponding values for the B profile are 19.9 and 12.0 kcal/mol, respectively. Hence, it turns out that the anticatalytic effect in the QM/MM calculations is mainly due to unfavorable interactions between the QM region and the surrounding MM region, as well as to the rearrangement of the MM region. Note also that the E_{QM} values in Table S5 in the Supporting Information are not far from those obtained in the gas-phase QM calculations (see Table S2 in the Supporting Information), especially in the case of the A configuration. This shows that the intrinsic stability of the QM region is influenced quite moderately by environmental effects.

Either QM/MM or QM calculations predict that the energy barrier for the initial nucleophilic attack is rather low (∼11−16 kcal/mol), which is clearly in consonance with the pre-reactive character of the enzyme/substrate contacts all along the MD simulation and in the QM/MM optimized **C_1** and **C_2** structures. However, protonation of the Ile(P_1')−N atom requires that the peptide substrate approaches the Glu_{404} group to accept a proton, a movement that is partially impeded in the static enzyme. These restrictions on the motion of the peptide substrate explain well the observed destabilization of the static QM/MM energy profiles with respect to the gas-phase QM results.

Comparison between the A and B QM/MM Profiles. As previously mentioned, the starting snapshot for the A profile is characterized by the presence of one water molecule interacting with the carbonyl group of the Gly(P_1) residue (Wat_2 in Figure 2). The corresponding H-bond interactions are preserved in all the QM/MM optimized structures. For the B profile, Wat_2 is missing, and no other H-bond interactions replace the lost water bridge between Pro_{423} and Gly(P_1). By comparing the A and B QM/MM profiles shown in Figure 3, it seems that the presence of Wat_2 favors the different reactive events along the reaction coordinate by lowering the energy profile in 5−15 kcal/mol depending on the critical point. In fact, Wat_2 influences both the interaction between the QM and MM regions, as well as the intrinsic stability of the QM region. For example, the global change between the A and B relative energies of **TS_3** (+10.0 kcal/mol) can be decomposed into +7.5 kcal/mol coming from the QM region (from E_{QM} values in Table S5 in the Supporting Information) and +2.5 kcal/mol corresponding to QM-MM and MM terms (from $E_{QM/MM}^{enzyme+solvent}$ values). Furthermore, the QM energy difference arises mainly from the intrinsic stability of the **TS_3** structures given that the QM energy differences (ΔE_{QM}) for the formal processes **C_1**(*A*) → **C_1**(*B*) and **TS_3**(*A*) → **TS_3**(*B*) amount to 1.0 and 8.6 kcal/mol, respectively. This means that the direct interaction between the QM region and Wat_2 cannot explain the energy differences between the A and B profiles.

Regardless of the relatively large changes in the QM/MM energies, the internal geometry of the reactive atoms in the A and B models barely changes (see Table S4 in the Supporting Information). In terms of the bond distances and the bond angles involving the reactive atoms (e.g., $Gly(P_1)-C\cdots N-Ile(P_1')$, $Wat_1-H2\cdots N-Ile(P_1')$, etc.), the equivalent transition structures and intermediates in the two reaction profiles exhibit only minor differences of ±0.02 Å and ±1 deg, respectively, thus supporting the assessment that the transition structures and intermediates in the MMP-2 mechanism are quite stable molecular entities. Nevertheless, a closer inspection of all the geometrical data reveals that Wat_2 could act as a molecular wedge to slightly increase the separation of the peptide substrate and the MMP-2 Ω-loop. For instance, the $Ile_{424}-C\cdots C\gamma-Ile(P_1')$ distance is reduced from 4.23 Å at **TS_3**(A) to 3.76 Å at **TS_3**(B). In this way, we see that in the A configuration, the steric restrictions on the motion of the peptide substrate are partially relaxed, and a better contact between the Ile(P_1') amino group and the catalytic Glu_{404} side chain results, as measured by the $Glu_{404}-O\varepsilon 2\cdots N-Ile(P_1')$ distance, which is 0.3−0.03 Å shorter. Similarly, the Glu_{404} carboxylate group and the scissile C−N bond are closer to coplanarity in the A configuration, as measured by the values of the dihedral angle defined by the Gly(P_1)−C, Ile(P_1')−N•, $Glu_{404}-O\varepsilon 2$•, and $Glu_{404}-C\delta$ atoms (see Table S4 in the Supporting Information).

Role of Structural Fluctuations: MM-PB Calculations and Approximate free energy Profiles. In principle, the impact of the steric hindrance observed in the QM/MM energy profiles is likely overestimated because most of the protein and solvent molecules remain fixed during the QM/MM geometry optimizations, and energy minimization methodologies are not as effective as MD approaches in dealing with intraprotein and protein−substrate interactions. On the basis that the structural

features of the A and B reaction paths determined by the QM/MM calculations are essentially the same (apart from small differences in the relative position between the Gly(P_1)∼Ile(P_1') peptide bond and the Glu_{404} carboxylate group), it can be reasonably expected that the internal geometry of the reaction path would not be substantially altered upon inclusion of dynamical environmental effects. In this way, the energetic effects of structural fluctuations on the QM/MM energy profiles can be estimated by means of the MM-PB computational scheme, as described in the Experimental Methods section.

For each of the QM/MM optimized structures in the A and B profiles, we generated MM representations for their respective QM regions within the context of the AMBER force field. The combined performance of the MM-PB calculations and the resulting MM models for studying environmental effects on the MMP-2 hydrolysis reaction was assessed by carrying out single-point MM-PB calculations on the same A and B snapshots that were used in the QM/MM geometry optimizations. Then, the energies of the QM region (E_{QM}) for the different critical points are combined with their single-point MM-PB free energy corrections $\Delta G_{MMPB}^{single\text{-}point}$, and the results are compared with QM/MM energies complemented with PB calculations, $E_{QM/MM}^{enzyme} + G_{PB}$. Note that the basic difference between the two sets of energetic data lies in the methodology employed to account for the interaction between the QM region and the rest of the enzymatic system. The mean unsigned energy differences between the $E_{QM} + \Delta G_{MMPB}^{single\text{-}point}$ and the $E_{QM/MM}^{enzyme} + G_{PB}$ energies are only 0.7 and 1.0 kcal/mol for the A and B profiles, respectively. In addition, we see in Figure 3 that the test MM-PB energy profiles (hollow triangles and brown lines) match quite well the QM/MM data (filled circles and magenta lines) all along the reaction coordinate. Hence, we conclude that our MM-PB calculations on the MMP-2 system give descriptions of environmental effects similar to those provided by the QM/MM calculations.

Starting at the A and B snapshots, we carried out two 5.0 ns MD simulations by using the LES technique to sample the most likely enzyme and solvent conformations in the presence of MM representations corresponding to the $\mathbf{C_1}$, $\mathbf{I_1}$, $\mathbf{I_2}$, $\mathbf{I_3}$, and **P** structures (the LES copies). All the relevant H-bond and hydrophobic contacts for substrate binding that have been observed in the previous simulations of the Michaelis complexes were preserved during the MD-LES simulations. Similarly, the $Gly(P_1)-O\cdots Wat_2\cdots O-Pro_{423}$ water bridge was observed in a small percentage (2%) of the analyzed MD-LES snapshots. The MM-PB energy calculations for the A and B profiles were done on 100 snapshots extracted from the second half of the corresponding trajectories. The average values of the MM-PB free energy corrections, which have a statistical imprecision below 0.4 kcal/mol in terms of standard errors, were combined with the QM energies of the reactive region in order to obtain the approximate free energy profiles in the MMP-2 enzyme ($E_{QM} + \Delta\bar{G}_{MMPB}$data in Table S5 in the Suporting Information).

Most interestingly, the MD-LES and MM-PB calculations show that the protein and solvent environment is well adapted to accommodate all the reactive structures involved in the MMP-2 hydrolysis reaction thanks to structural fluctuations of residues and water molecules located in the vicinity of the active site. Thus, we see in Figure 3 that the relative free energies are lower than the static QM/MM ones by 5−12 kcal/mol depending on the critical point. This suggests that the enzyme structures used in the QM/MM energy minimizations are partially biased toward the pre-reactive Michaelis complex, which in turn results in the somewhat artificial steric constraints on the peptide substrate which seem to destabilize the concluding stages of the reaction. The MD-LES simulations overcome this problem by generating an unbiased ensemble of enzyme/substrate configurations that are equally compatible with all the reactive structures. Moreover, the subsequent MM-PB calculations indicate that the MMP-2 enzymatic environment can actually play a catalytic role. For the B profile, addition of the relative $\Delta\bar{G}_{MMPB}$ values to the corresponding E_{QM} values results in a net stabilization of the energy profile by 2−3 kcal/mol (see Table S5 in the Suporting Information and Figure 3), which stems from nonbonding electrostatic interactions as revealed by the analysis of the MM-PB energy components (data not shown for brevity). The MM-PB free energy corrections for the A profile have a similar stabilizing effect on the nucleophilic attack but a small anticatalytic effect on the $Glu_{404} \rightarrow Ile(P_1')$ proton transfer and on the peptide cleavage due to van der Waals interactions. Both the A and B MM-PB free energy profiles consistently predict that the rate-determining events in the MMP-2 mechanism would correspond to the H-bond rearrangement involving the Glu_{404} residue and the $Glu_{404}-COOH \rightarrow Ile(P_1')-N$ proton transfer described by the $\mathbf{TS_2} \rightarrow \mathbf{I_2} \rightarrow \mathbf{TS_3}$ structures.

Removal of the steric hindrance observed in the QM/MM energy profiles through the MM-PB free energy corrections reduces significantly the energetic differences between the A and B profiles. Thus, the free energy barriers for the A and B profiles are now 13.2 ($\mathbf{TS_3}$) and 18.3 ($\mathbf{TS_2}$) kcal/mol, respectively, which seem both quite reasonable. Note that this effect arises only from the dynamical fluctuations around the reactive region and does not depend on the presence or absence of the bridging water molecule between the Gly(P_1) and the Pro_{423} carbonyl groups given that this water bridge exits only in about 2% of the MD-LES snapshots. Because the internal geometry of the A structures is more relaxed than that of the B structures and all the A structures are compatible with the structural fluctuations of the surrounding environment, we conclude that the QM/MM structures and the free energy profile for the A configuration should be considered as the most likely representation of the catalytic MMP-2 mechanism.

Finally, we can estimate the vibrational free energy contributions arising from the reactive QM atoms, which are not considered in the MM-PB approach, on the basis of the harmonic free energy corrections that were computed by using the B3LYP/LACVP* Hessian matrices of the gas-phase QM structures. Addition of the vibrational free energy correction of the gas-phase $^{QM}\mathbf{TS_2}$ structure (1.6 kcal/mol) to the $E_{QM} + \Delta\bar{G}_{MMPB}$ energy of the rate-determining $\mathbf{TS_3}$ structure in the A configuration (13.2 kcal/mol) gives our best prediction for the total free energy barrier: 14.8 kcal/mol.

Comparison with Previous Theoretical Results. As mentioned in the Introduction, Pelmenschikov and Siegbahn have used QM methodologies to investigate the hydrolysis of *N*-methyl-acetamide catalyzed by a cluster model of the MMP-3 enzyme.[26] According to their free energy profile, the reaction proceeds through a single-step mechanism in which the rate-determining event corresponds to the initial nucleophilic attack with a ΔG value of 13.1 kcal/mol. The authors show that the transition structure would be connected with a *gem*-diolate intermediate similar to the $^{QM}\mathbf{I_2}$ structure in Figure 1. However, in terms of free energy, this intermediate would be a transient species, which evolves readily toward products through the barrierless rupture of the amide C−N bond. Hence, these former calculations did not provide any structural or energetic details about the rearrangement of the glutamic acid and/or the

protonation of the leaving amino group, which would be the rate determining events according to our results. Most likely, the differences between the previous QM data and the present results stem from the limited representation of the protein environment in the former calculations. With respect to the model of Pelmenschikov and Siegbahn, our calculations point out that the enzymatic environment contributes to properly orient the peptide substrate in the active site, thus facilitating the nucleophilic attack, and simultaneously, the placement of the Ile(P_1') side chain inside the S_1' pocket hinders the approach of the Ile(P_1')−N atom to the Glu_{404} carboxylate, thus increasing the energy barrier for the protonation of the leaving amino group. Therefore, although it is true that the peptidase machinery is essentially provided by the Zn_1-binding motif, a more reliable analysis of the catalysis exerted by the MMP enzymes requires the explicit consideration of the whole catalytic domain.

In their recent work,[12] Bertini et al. have described a sequence of reactive events in the active site of the MMPs on the basis of the X-ray structure of the active (unbound) MMP-12 enzyme, a computational model of a tetrahedral *gem*-diol intermediate formed between the MMP-12 enzyme and the Pro−Gln−Gly∼-Ile−Ala−Gly hexapeptide, and two more crystallographic structures: the MMP-12 adduct with both the Pro−Gln−Gly and Ile−Ala−Gly peptides and the adduct of MMP-12 with only one peptide (Ile−Ala−Gly). Visual inspection of the *gem*-diol intermediate of Bertini et *al.* shows that this structure is readily comparable to the $^{QM}\mathbf{I_1}$ and $\mathbf{I_1}$ critical points in Figures 1 and 2; that is, the Zn_1 ion retains five-coordination, the catalytic Glu is H-bonded with one of the oxygen atoms coordinated to Zn_1, and so forth. We note that our QM/MM optimized structures complement the structures of Bertini et al. by providing further energetic and structural details of the nucleophilic attack leading to the *gem*-diol intermediate and its subsequent evolution toward the product complex. On the other hand, the experimental structures of the two MMP-12 adducts with the tripeptides provide important information concerning product release that is not accessible to our QM/MM calculations. As noticed by Bertini et al., in the X-ray structures, a water molecule is placed between the Zn_1-bound carboxylate and the catalytic Glu residue that could facilitate the release of the Pro−Gln−Gly fragment through an associative ligand exchange mechanism. The structures of Bertini et al. have also revealed that the second peptide fragment, Ile−Ala−Gly, remains more strongly bound within the S_1' pocket of the enzyme site. Therefore, the computational QM/MM snapshots together with the experimental ones complement each other to provide a more detailed view of the MMPs catalytic mechanism.

Comparison with Kinetic Experimental Data. Overall, our calculations on the MMP-2 mechanism are in consonance with experimental kinetic data available for different MMP enzymes. Thus, our best prediction for the free energy barrier, 14.8 kcal/mol, is in good agreement with experimental results on the reaction between the MMP-2 enzyme and a fluorogenic substrate (MCA−Pro−Leu−Gly∼Leu−DPA−Ala−Arg−NH_2) that is similar to the **Pα1** substrate studied in this work at the level of the scissile peptide bond. In this case, the analysis of the temperature dependence of the kinetic parameter k_{cat} resulted in a $\Delta G^{\ddagger}$ value of 15.4 ± 1.0 kcal/mol at pH 7.0 and 37 °C.[51] On the other hand, the kinetic parameters for the MMP-2 catalyzed hydrolysis of several octapeptides, including the **Pα1** substrate, have been reported at 30 °C.[15] By using the classical TS formula, the experimental k_{cat} constant for the hydrolysis of **Pα1** (9700 h^{-1}) results in an activation free energy barrier of 17.1 kcal/mol, which again compares reasonably well with the computed value.

Quite remarkably, all the calculations reported in this work, QM, QM/MM, and the approximate QM-MMPB free energy calculations, point out that the hydrolysis reaction catalyzed by MMP-2 takes place through what is, essentially, a single-step mechanism given that the corresponding energy basins around the different tetrahedral intermediates are quite shallow. In this way, tetrahedral intermediates would not accumulate to an experimentally detectable amount, which is in agreement with the lack of experimental evidence for the existence of stable intermediates in the hydrolysis of peptide substrates by the MMPs.[15,52] For the MMP-2 enzyme, the broad maximum along the free energy profile occurs at the formation of the Glu_{404}−COOH···N−Ile(P_1') H-bond interaction and the protonation of the N atom as described by the nearly isoenergetic $\mathbf{TS_2} \rightarrow \mathbf{I_2} \rightarrow \mathbf{TS_3}$ structures. These observations are also in consonance with experimental data on kinetic solvent isotope effects for the hydrolysis reaction of the Dnp−Pro−Leu−Gly∼Leu−Trp−Ala−D−Arg−NH_2 peptide assisted by the MMP-2 enzyme. The reported value for the $k_{cat,H_2O}/k_{cat,D_2O}$ ratio amounts to 1.5, thus suggesting that a proton is being transferred between electronegative atoms at the rate-limiting step of the reaction mechanism.[17] According to our results, this kinetic solvent isotope effect is most likely due to the proton transfer between Glu_{404} and the leaving amino group of the peptide substrate as characterized by the $\mathbf{TS_3}$ structure, in which the reactive H atom is located at 1.2 and 1.4 Å from the Glu_{404}−Oε2 and the Ile(P_1')−N atoms, respectively.

The fact that the rate-determining events correspond to the Glu_{404} → N−Ile(P_1') proton transfer and/or the rearrangement of the H-bond network around Glu_{404} as described by our calculations (see Figure 2) can help interpret the mutagenesis experiments at the Glu_{404} residue. Thus, it has been reported that the Glu_{404} → Asp mutant of MMP-2 retains 10% of the wild-type activity against a synthetic substrate.[20] A similar decrease in activity has been observed in mutagenesis experiments in other MMP enzymes, showing that impact on activity is essentially due to a decrease in k_{cat}. Although the Asp carboxylate group at the 404 position could still act as a proton shuttle, it is clear that the shortening of the amino acid side chain would increase the energetic penalty of the approach of the peptide substrate toward the catalytic carboxylic group. In consonance with its mechanistic role, mutation of Glu_{404} by neutral residues (Ala or Gln) that eliminate acid/base properties reduces drastically the catalytic activity of the mutant enzymes (e.g., 0.01% that of the wild-type enzymes in the case of the MMP-2 enzymes).[20] We propose that these mutant enzymes might retain a low level of activity thanks to an auxiliary water molecule that could participate in a proton relay process from the Zn_1−Wat moiety to the leaving N atom concomitant with the nucleophilic attack on the peptide substrate.

Comparison with Zinc Binding Groups of MMP Inhibitors. In the substrate-based approach for the rational design of inhibitors against MMPs,[2] a fragment mimicking a preferred peptide substrate is usually attached to a zinc-binding group (ZBG) that chelates the catalytic Zn_1 ion by using oxygen or sulfur atoms. To this end, different ZBGs have been employed, namely, hydroxamates (−$CONHO^-$), carboxylate (−COO^-), thiolate (−S^-), and phosphinyl (−PO_2^-). Among all the ZBGs, hydroxamate binds most potently to the MMPs, and accordingly, most of the MMP inhibitors tested by pharmaceutical companies belong to this category. The high pK_a of hydroxamate helps it to transfer a proton to the active-site glutamic acid (Glu_{404} in

TABLE 1: RMSD (in Angtroms) for the $His_{403}-N\varepsilon$, $His_{407}-N\varepsilon$, $His_{413}-N\varepsilon$, Glu_{404}-Oε1, $Glu_{404}-O\varepsilon2$, Zn_1, Wat_1-O, $Gly(P_1)-C$, and $Gly(P_1)-O$ Atoms in the Different Critical Points and the Corresponding Atoms in Selected MMP/Inhibitor Complexes

rmsd	1HFC[a]	1JAP[b]	1I76[c]
$\mathbf{C_1}$	0.44	0.63	0.48
$\mathbf{C_2}$	0.46	0.62	0.48
$\mathbf{TS_1}$	0.36	0.63	0.28
$\mathbf{I_1}$	0.35	0.64	0.22
$\mathbf{TS_2}$	0.28	0.69	0.27
$\mathbf{I_2}$	0.32	0.73	0.35
$\mathbf{TS_3}$	0.33	0.74	0.35
$\mathbf{I_3}$	0.34	0.73	0.38
$\mathbf{TS_4}$	0.35	0.72	0.38
P	0.40	0.62	0.37

[a] MMP-1 with a hydroxamate inhibitor bound to the primed site (1.56 Å, K_i = 7 nM). [b] MMP-8 with a hydroxamate inhibitor bound to the unprimed site (1.82 Å, K_i = 19000 nM). [c] MMP-8 with a carboxylate inhibitor bound to the primed site (1.20 Å, K_i = 10 nM).

MMP-2) and results in bidentate complexes characterized by a distorted trigonal bipyramidal geometry around Zn_1.[53] The second best potency is achieved by reverse hydroxamates, followed by carboxylates, thiols, and phosphinyls.[7]

Our previous MD simulations of the Michaelis complex formed between the MMP-2 catalytic domain and the **Pα1** octapeptide have been useful to assess the relative importance of the H-bond and hydrophobic contacts between the peptide substrate and the different MMP-2 binding sites.[11] Similarly, the present QM/MM calculations of the Michaelis complexes and the rest of critical structures provide accurate structural parameters of the Zn_1 coordination shell that could be useful to better characterize the role of the ZBG in the MMPs inhibitors. To this end, we obtained the rmsd of the Zn_1-coordinating atoms and other selected atoms in three X-ray structures of MMPs inhibited by hydroxamate and carboxylate compounds, with respect to the QM/MM optimized structures in the A configuration (see Table 1). Thus, we see in Table 1 that the carboxylate and hydroxamate ZBGs of two primed-site inhibitors (PDB ID codes 1I76 and 1HFC, respectively) match quite well the coordination environment around Zn_1 all along the reaction pathway (rmsd values lower than 0.3−0.4 Å). In contrast, the hydroxamate ZBG of the inhibitor bound to the unprimed sites (1JAP), which shows only a modest inhibitory potency, exhibits larger rmsd values (0.6−0.7). These observations suggest that the Zn_1 mode of binding of the unprimed inhibitors would be less efficient than that of the primed ones. Nevertheless, it has been noticed that the non-primed positions of peptidomimetic inhibitors play a key role in substrate specificity across the MMP family of enzymes. Therefore, we believe that the MD-LES simulations on the MMP-2/**Pα1** complex, as well as further computational data derived for other MMPs using similar computational protocols, could provide new guidelines useful in the design of specific and potent inhibitors by describing all the enzyme−substrate interactions at the different stages of the catalytic mechanism.

Conclusions

On the basis of the QM and QM/MM energy optimizations as well as the MD-LES simulations complemented with the subsequent MM-PB free energy calculations that are reported in this work, we can draw the following conclusions relevant to the reaction mechanism for peptide hydrolysis catalyzed by the MMP-2 enzyme.

(a) In consonance with previous proposals, we confirm that a Zn_1-bound water molecule attacks the carbonyl group of the scissile peptide bond with the assistance of the conserved Glu_{404} residue that, subsequently, shuttles a proton to the leaving amino group. For this mechanism, the optimized QM and QM/MM critical structures provide much detailed structural information: the pre-reactive complex is well pre-organized for nucleophilic attack, the Zn_1 ion remains five-coordinated along the reaction mechanism, the side chain of the Ile(P_1') shifts toward the Glu_{404} side chain, and so forth. The internal geometry of the transition structures and intermediates is quite stable against small changes in the environment.

(b) According to the different energy calculations, the catalytic reaction follows essentially a single-step mechanism given that tetrahedral intermediates would not accumulate to an experimentally detectable amount. The computed free energy barrier (14.8 kcal/mol) is determined by the H-bond rearrangement around the Glu_{404} residue and the $Glu_{404}-COOH \rightarrow N-Ile(P_1')$ proton transfer.

(c) Although the static QM/MM calculations yield a detailed reaction path, the rigidity of the protein and solvent environment during energy minimizations results in an energetic bias toward the first critical structures, thus destabilizing the latter stages of the reaction. This limitation is overcome by means of the MD-LES and MM-PB calculations, showing that structural fluctuations of the active site are able to accommodate well all the reactive structures involved in the MMP-2 hydrolysis reaction.

(d) The computationally derived structures and relative energies complement nicely the previous structural information by Bertini et al.,[12] and altogether, they provide a more detailed movie of the catalytic cycle. In addition, the computational results are not only compatible with kinetic experimental data (e.g., k_{cat} constants) but help interpret some experimental results about the mutagenesis of the Glu_{404} residue and kinetic solvent isotope effects.

(e) The Zn_1 mode of binding of the primed hydroxamate inhibitors resembles closely that observed in the optimized QM/MM structures. A worse match is observed for the unprimed hydroxamate inhibitors, thus suggesting that these compounds bind to the Zn_1 site less efficiently.

Finally, we note that the present results about the MMP-2 reaction mechanism together with the previous MD study on the Michaelis complex could be useful to better understand the thermodynamic and kinetic preferences of peptide substrates and/or peptido-mimetic inhibitors of the different MMP enzymes.

Acknowledgment. This research was supported by the Spanish MEC via the "Ramon y Cajal" program and Grant CTQ2004-06309.

Supporting Information Available: Validation calculations (Table S1 and Figure S1). Energy components from the QM (Table S1) and QM/MM (Table S5) geometry optimizations. QM/MM structures for configuration B (Figure S2). Superposition of the peptide substrate along the QM and QM/MM optimizations (Figure S3). Geometrical parameters from the QM/MM optimizations (Tables S3 and S4). This material is available free of charge via de Internet at http://pubs.acs.org.

References and Notes

(1) Shapiro, S. D. *Curr. Opin. Cell Biol.* **1998**, *10*, 602.

(2) Whittaker, M.; Floyd, C. D.; Brown, P.; Gearing, A. J. H. *Chem. Rev.* **1999**, *99*, 2735.
(3) Sternlicht, M. D.; Werb, Z. *Annu. Rev. Cell Dev. Biol.* **2001**, *17*, 463.
(4) Overall, C. M.; Kleifeld, O. *Nat. Rev. Cancer* **2006**, *6*, 227.
(5) Fingleton, B. *Curr. Pharm. Design* **2007**, *13*, 333.
(6) Cuniasse, P.; Devel, L.; Makaritis, A.; Beau, F.; Georgiadis, D.; Matziari, M.; Yiotakis, A.; Dive, V. *Biochimie* **2005**, *87*, 393.
(7) Rao, B. G. *Curr. Pharm. Design* **2005**, *11*, 295.
(8) Overall, C. M.; Kleifeld, O. *Br. J. Cancer* **2006**, *94*, 941.
(9) Nuti, E.; Tuccinardi, T.; Rossello, A. *Curr. Pharm. Design* **2007**, *13*, 2087.
(10) Maskos, K. *Biochimie* **2005**, *87*, 249.
(11) Díaz, N.; Suárez, D. *Proteins: Struct., Funct., Bioinf.* **2008**, *72*, 50–61.
(12) Bertini, I.; Calderone, V.; Fragai, M.; Luchinat, C.; Maletta, M.; Yeo, K. J. *Angew. Chem., Int. Ed.* **2006**, *45*, 7952.
(13) Díaz, N.; Suárez, D.; Sordo, T. L. *J. Phys. Chem. B* **2006**, *110*, 24222.
(14) Netzel-Arnett, S.; Fields, G.; Birkedal-Hansen, H.; Van Wart, H. E. *J. Biol. Chem.* **1991**, *266*, 6747.
(15) Netzel-Arnett, S.; Sang, Q.-X.; Moore, W. G. I.; Navre, M.; Birkedal-Hansen, H.; Van Wart, H. E. *Biochemistry* **1993**, *32*, 6427.
(16) Chen, E. I.; Li, W.; Godzik, A.; Howard, E. W.; Smith, J. W. *J. Biol. Chem.* **2003**, *278*, 17158.
(17) Stack, M. S.; Gray, R. D. *Arch. Biochem. Biophys.* **1990**, *281*, 257.
(18) Cha, J.; Auld, D. S. *Biochemistry* **1997**, *36*, 16019.
(19) Johnson, L. L.; Pavlovsky, A. G.; Johnson, A. R.; Janowicz, J. A.; Man, C.-F.; Ortwine, D. F.; Purchase, C. F.; White, A. D. *J. Biol. Chem.* **2000**, *275*, 11026.
(20) Crabbe, T.; Zucker, S.; Cockett, M. I.; Willenbrock, F.; Tickle, S.; O'Connell, J. P.; Scothem, J. M.; Murphy, G.; Docherty, A. J. P. *Biochemistry* **1994**, *33*, 6684.
(21) Windsor, L. J.; Bodden, M. K.; Birkedal-Hansen, B.; Engler, J. A.; Birkedal-Hansen, H. *J. Biol. Chem.* **1994**, *269*, 26201.
(22) Arza, B.; De Maeyer, M.; Félez, J.; Collen, D.; Lijnen, H. R. *Eur. J. Biochem.* **2001**, *268*, 826.
(23) Matthews, B. W. *Acc. Chem. Res.* **1988**, *21*, 333.
(24) Blumberger, J.; Lamoureux, G.; Klein, M. L. *J. Chem. Theory Comput.* **2007**, *3*, 1837.
(25) Browner, M. F.; Smith, W. W.; Castelhano, A. L. *Biochemistry* **1995**, *34*, 6602.
(26) Pelmenschikov, V.; Siegbahn, P. E. M. *Inorg. Chem.* **2002**, *41*, 5659.
(27) Nguyen, M.; Arkell, J.; Jackson, C. J. *Int. J. Biochem. Cell Biol.* **2001**, *33*, 960.
(28) Turpeenniemi-Hujanen, T. *Biochimie* **2005**, *87*, 287.
(29) Díaz, N.; Suárez, D. *Biochemistry* **2007**, *46*, 8943.
(30) Gioia, M.; Fasciglione, G. F.; Marini, S.; D'Alessio, S.; De Sanctis, G.; Diekmann, O.; Pieper, M.; Politi, V.; Tschesche, H.; Coletta, M. *J. Biol. Chem.* **2002**, *277*, 23123.
(31) Aimes, R. T.; Quigley, J. P. *J. Biol. Chem.* **1995**, *270*, 5872.
(32) Morgunova, E.; Tuuttila, A.; Bergmann, U.; Isupov, M.; Lindqvist, Y.; Schneider, G.; Tryggvason, K. *Science* **1999**, *284*, 1667.
(33) Hehre, W. J.; Ditchfield, R.; Pople, J. A. *J. Chem. Phys.* **1972**, *62*, 2257.
(34) Hay, P. J.; Wadt, W. R. *J. Chem. Phys.* **1985**, *82*, 299.
(35) *JAGUAR*, 5.5 ed.; Schrödinger, L.LC.: Portland, OR, 1991−2003.
(36) Frisch, M. J.; Trucks, G. W.; Schlegel, H. B.; Scuseria, G. E.; Robb, M. A.; Cheeseman, J. R.; Montgomery, J. A., Jr.; Vreven, T.; Kudin, K. N.; Burant, J. C.; Millam, J. M.; Iyengar, S. S.; Tomasi, J.; Barone, V.; Mennucci, B.; Cossi, M.; Scalmani, G.; Rega, N.; Petersson, G. A.; Nakatsuji, H.; Hada, M.; Ehara, M.; Toyota, K.; Fukuda, R.; Hasegawa, J.; Ishida, M.; Nakajima, T.; Honda, Y.; Kitao, O.; Nakai, H.; Klene, M.; Li, X.; Knox, J. E.; Hratchian, H. P.; Cross, J. B.; Bakken, V.; Adamo, C.; Jaramillo, J.; Gomperts, R.; Stratmann, R. E.; Yazyev, O.; Austin, A. J.; Cammi, R.; Pomelli, C.; Ochterski, J. W.; Ayala, P. Y.; Morokuma, K.; Voth, G. A.; Salvador, P.; Dannenberg, J. J.; Zakrzewski, V. G.; Dapprich, S.; Daniels, A. D.; Strain, M. C.; Farkas, O.; Malick, D. K.; Rabuck, A. D.; Raghavachari, K.; Foresman, J. B.; Ortiz, J. V.; Cui, Q.; Baboul, A. G.; Clifford, S.; Cioslowski, J.; Stefanov, B. B.; Liu, G.; Liashenko, A.; Piskorz, P.; Komaromi, I.; Martin, R. L.; Fox, D. J.; Keith, T.; Al-Laham, M. A.; Peng, C. Y.; Nanayakkara, A.; Challacombe, M.; Gill, P. M. W.; Johnson, B.; Chen, W.; Wong, M. W.; Gonzalez, C.; Pople, J. A. *Gaussian 03*, revision C.02; Gaussian, Inc.: Wallingford, CT, 2004.
(37) Tannor, D. J.; Marten, B.; Murphy, R.; Friesner, R. A.; Sitkoff, D.; Nicholls, A.; Ringnalda, M.; Goddard, I., W. A.; Honig, B. *J. Am. Chem. Soc.* **1994**, *116*, 11875.
(38) *Qsite*; Schrodinger, Inc.: Portland, OR, 2000.
(39) Kaminski, G. A.; Friesner, R. A.; Tirado-Rives, J.; Jorgensen, W. L. *J. Phys. Chem. B* **2001**, *105*, 6474.
(40) Murphy, R. B.; Philipp, D. M.; Friesner, R. A. *J. Comput. Chem.* **2000**, *21*, 1442.
(41) Rocchia, W.; Alexov, E.; Honig, B. *J. Phys. Chem. B* **2001**, *105*, 6507.
(42) Case, D. A.; Darden, T. A.; Cheatham, I., T. E.; Simmerling, C. L.; Wang, J.; Duke, R. E.; Luo, R.; Merz, K. M.; Pearlman, D. A.; Crowley, M.; Walker, R. C.; Zhang, W.; Wang, B.; Hayik, S.; Roitberg, A.; Seabra, G.; Wong, K. F.; Paesani, F.; Wu, X.; Brozell, S.; Tsui, V.; Gohlke, H.; Yang, L.; Tan, C.; Mongan, J.; Hornak, V.; Cui, G.; Beroza, P.; Mathews, D. H.; Schafmeister, C.; Ross, W. S.; Kollman, P. A. *AMBER 9*; University of California: San Francisco, 2006.
(43) Gao, J.; Ma, S.; Major, D. T.; Nam, K.; Pu, J.; Truhlar, D. G. *Chem. Rev.* **2006**, *106*, 3188.
(44) Kollman, P. A.; Kuhn, B.; Donini, O.; Perakyla, M.; Stanton, R.; Bakowies, D. *Acc. Chem. Res.* **2001**, *34*, 72.
(45) Elber, R.; Karplus, M. *J. Am. Chem. Soc.* **1990**, 9161.
(46) Kollman, P. A.; Massova, I.; Reyes, C.; Kuhn, B.; Huo, S.; Chong, L.; Lee, M.; Lee, T.; Duan, Y.; Wang, W.; Donini, O.; Cieplak, P.; Srinivasan, J.; Case, D. A.; Cheatham, T. E. *Acc. Chem. Res.* **2000**, *33*, 889.
(47) Suarez, D.; Diaz, N.; Fontecilla-Camps, J.; Field, M. J. *Biochemistry* **2006**, *45*, 7529.
(48) Rosta, E.; Klähn, M.; Warshel, A. *J. Phys. Chem. B* **2006**, *110*, 2934.
(49) Bayly, C. A.; Cieplak, P.; Cornell, W. D.; Kollman, P. A. *J. Phys. Chem.* **1993**, *97*, 10269.
(50) Rappé, A. K.; Casewit, C. J.; Colwell, K. S.; Goddard, W. A., III; Skiff, W. M. *J. Am. Chem. Soc.* **1992**, *114*, 10024.
(51) Fasciglione, G. F.; Marini, S.; D'Alessio, S.; Politi, V.; Coletta, M. *Biophys. J.* **2000**, *79*, 2138.
(52) Chen, E. I.; Kridel, S. J.; Howard, E. W.; Li, W.; Godzik, A.; Smith, J. W. *J. Biol. Chem.* **2002**, *277*, 4485.
(53) Cross, J. B.; Duca, J. S.; Kaminski, J. J.; Madison, V. S. *J. Am. Chem. Soc.* **2002**, *124*, 11004.

JP803509H